Modulation of a μ-1,2-Peroxo Dicopper(II) Intermediate by Strong Interaction with Alkali Metal Ions

Alexander Brinkmeier,[†,$] Kristian E. Dalle,[†,$,#] Lorenzo D'Amore,[Ψ,$] Roland A. Schulz,[†] Sebastian Dechert,[†] Serhiy Demeshko,[†] Marcel Swart,*[,Ψ,§] and Franc Meyer*[,†,‡]

[†] University of Göttingen, Institute of Inorganic Chemistry, Tamannstrasse 4, D-37077 Göttingen, Germany
[Ψ] Institut de Química Computacional i Catàlisi (IQCC) & Dept. Química, Universitat de Girona, 17003 Girona, Spain
[§] ICREA, Pg. Lluís Companys 23, 08010 Barcelona, Spain
[‡] University of Göttingen, International Center for Advanced Studies of Energy Conversion (ICASEC), D-37077 Göttingen, Germany

[$] These authors contributed equally to the work
[#] new address: Australian Catholic University - Brisbane Campus, 1100 Nudgee Road, Banyo, Brisbane, QLD, 4014, AUS

Abstract. The properties of metal-dioxygen species, which are key intermediates in oxidation catalysis, can be modulated by interaction with redox-inactive Lewis acids, but structural information about these adducts is scarce. Here we demonstrate that even mildly Lewis acidic alkali metal ions, which are typically viewed as innocent 'spectators', bind strongly to a reactive *cis*-peroxo dicopper(II) intermediate. Unprecedented structural insight has now been obtained from X-ray crystallographic characterization of the 'bare' $Cu^{II}_2(\mu\text{-}\eta^1\text{:}\eta^1\text{-}O_2)$ motif and its Li^+, Na^+, and K^+ complexes. UV-vis, Raman and electrochemical studies show that the binding persists in MeCN solution, growing stronger in proportion to the cation's Lewis acidity. The affinity for Li^+ is surprisingly high (~7×10^4 M^{-1}), leading to Li^+ extraction from its crown ether complex. Computational analysis indicates that the alkali ions influence the entire Cu-OO-Cu core, modulating the degree of charge transfer from copper to dioxygen. This induces significant changes in the electronic, magnetic, and electrochemical signatures of the Cu_2O_2 species. These findings have far-reaching implications for analyses of transient metal/dioxygen intermediates, which are often studied *in situ*, and they may be relevant to many (bio)chemical oxidation processes when considering the widespread presence of alkali cations in synthetic and natural environments.

Introduction

Reactive intermediates formed upon metal-mediated activation of dioxygen, including superoxo, peroxo, or high-valent metal-oxo species, play key roles in many chemical and biochemical oxidative transformations.[1] It is now increasingly realized that the reactivity of these important intermediates can be modulated by interaction with additional redox-inactive metal ions that serve as Lewis acids.[2,3] Often cited as a prominent example from biology is the Ca^{2+} ion that is an integral component of nature's oxygen-evolving complex (OEC) in photosystem II, which contains a Mn_4CaO_5 core structure.[4] In molecular systems, strongly Lewis acidic metal ions such as Zn^{2+} or Sc^{3+} have been used to, inter alia, stabilize unusual oxocobalt(IV) complexes,[5] induce valence tautomerism in high-valent oxomanganese porphyrinoids for enhancing their reactivity,[6] or tune the redox reactivity of oxometal intermediates by enabling metal ion-coupled electron transfer (MCET).[7] Just recently, it was shown that reaction between a peroxocobalt(III) complex and nitriles leads to completely different products in the absence or presence of M^{n+} (M^{n+} = Zn^{2+}, La^{3+}, Lu^{3+}, or Y^{3+}).[8] As was also mentioned, however, the impact of the redox-active metal ion on the metal-peroxo intermediate remains underexplored, and the mechanism of action is poorly understood.[8] In particular, crucial structural information about these adducts between reactive metal-oxygen species and Lewis acids is scarce.

A crystallographically determined structure with a Fe-O-Sc motif, obtained from scandium triflate and the oxoiron(IV) species $[(TMC)Fe^{IV}(O)]^{2+}$ (TMC is tetramethylcyclam),[9] was later shown to contain Fe^{III}.[10] The iron(III) side-on peroxo complex $[(TMC)Fe^{III}(O_2)]^+$ was reported to bind various di- and tricationic redox-inactive metal ions to give adducts with a $\mu\text{-}\eta^2\text{:}\eta^2\text{-}O_2^{2-}$ group (**I**, Figure 1) based on DFT optimized structures and EXAFS analysis.[11] Electron transfer properties as well as electrophilic and nucleophilic reactivities of adducts **I** correlate with the Lewis acidity of the metal ion M,[12] and in the presence of electron donors the Lewis acid may promote O-O bond cleavage to trigger the formation of an oxoiron(IV) complex.[13] Similarly, Que et al. recently reported that a (μ-1,2-peroxo)diiron(III) intermediate undergoes O–O bond rupture upon treatment with the Lewis acid Sc^{3+}, transforming into a bis(μ-oxo)diiron(IV) complex.[14]

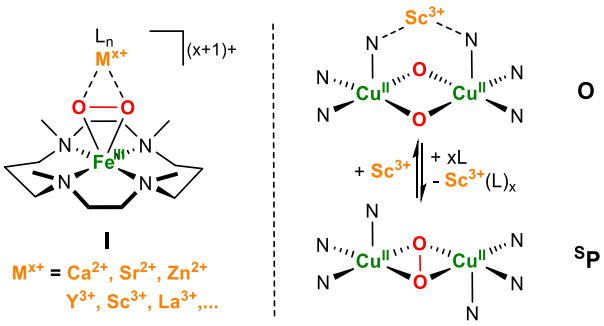

Figure 1. Lewis acid adducts of peroxo complex $[(TMC)Fe^{III}(O_2)]^+$ (left)[11] and reversible O–O cleavage interconverting ^{S}**P** and **O** cores in Cu_2O_2 intermediates mediated by the Lewis acid Sc^{3+} (right).[15]

In copper/dioxygen chemistry, O-O bond cleavage in some μ-η^2:η^2-peroxodicopper(II) (*side-on* peroxo, ^{S}**P**) complexes to give the corresponding bis(μ-oxo)dicopper(III) (**O**) species can also be triggered by Sc^{3+}; in this case, the redox-inert metal ion was shown to interact with N-donor groups of the ligands (Figure 1).[15] In

terms of reactivity of Cu/O_2 intermediates, Sc^{3+} was shown to induce a change from a four- to a two-electron mechanism in a Cu-catalyzed dioxygen reduction reaction.[16]

In most of the reported studies, including all of the abovementioned examples, moderately or strongly Lewis acidic di- and trivalent redox-inactive metal ions are used, most commonly Sc^{3+}. Adduct formation between reactive metal-oxygen intermediates and monocationic alkali metal ions has been much less evidenced, despite Na^+ and K^+ being abundant in biological systems and often being present in reaction mixtures in the laboratory. A notable example is the series of Cr^{III} superoxide complexes $[L_2Cr]M_2O_2(THF)_y$ (M^+ = Li^+, Na^+, K^+; L^{2-} is a disilanolate ligand) discovered by Limberg et al.,[17] in which isolation of the Cr^{III}-superoxide (obtained from the corresponding Cr^{II} complex and O_2) is assisted by end-on interaction of the superoxide with the alkali metal ion. The choice of M^+ was found to significantly influence the stability and reactivity of these complexes.

A few years ago we reported the first structurally authenticated *cis*-μ-η^1:η^1-peroxo (**^{C}P**) type dicopper(II) complex $[LCu^{II}_2(O_2)]^+$ (**1**; Figure 2) using a dinucleating pyrazolate/TACN hybrid ligand L^- (TACN = 1,4,7-triazacyclononane) that provides two {N_4} binding sites and a bimetallic pocket in which the reduced O_2 substrate is hosted with a Cu-O-O-Cu torsion angle of 65°.[18] The **^{C}P** motif differs from the more common *trans*-μ-η^1:η^1-peroxodicopper(II) (**^{T}P**) core (Figure 2), of which several crystallographically characterized examples are known,[19] and it is relevant for understanding the mechanism of O_2 reduction at type III dicopper metalloprotein active sites since it represents a snapshot of the proposed O_2 binding trajectory that ultimately leads to the **^{S}P** core.[20,21] The triflate salt of **1** was isolated after deprotonating the proligand HL with NaOtBu, adding two equivalents of $[Cu^I(MeCN)_4]OTf$ and subsequent oxygenation at -30°C. Interestingly, X-ray crystallography revealed a close *side-on* association of the Na^+ ion with the exposed *cis*-μ-η^1:η^1-peroxo unit,and titration experiments indicated that substantial affinity also persists in acetone solution (association constant K_a = 17 × 10^2 (± 10%) M^{-1}).[18]

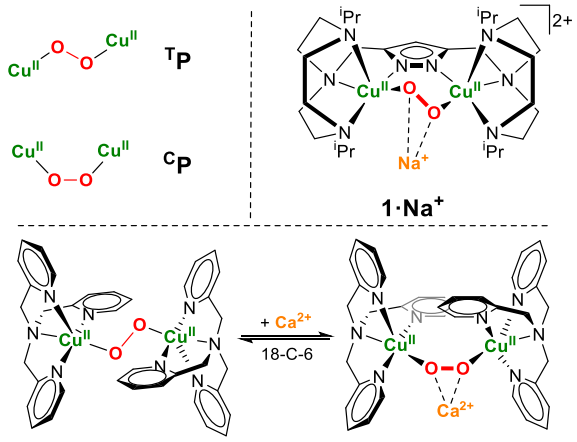

Figure 2. *trans* (**^{T}P**) and *cis* (**^{C}P**) μ-η^1:η^1-peroxodicopper(II) motifs (top left), structurally characterized **^{C}P** type complex **1·Na$^+$** that has a Na^+ associated with the μ-η^1:η^1-peroxo unit (top right),[18] and proposed interconversion between **^{T}P** and **^{C}P** forms of $\{[Cu^{II}(TMPA)]_2(\mu\text{-}1,2\text{-}O_2)\}^{2+}$ (bottom).[22]

Very recently, it was reported that Ca^{2+} mediates the transformation of the prototypical **^{T}P** species $\{[Cu^{II}(TMPA)]_2(\mu\text{-}1,2\text{-}O_2)\}^{2+}$ (TMPA = tris(2-pyridylmethyl)amine) to the corresponding **^{C}P** form (Figure 2, bottom), based on UV-vis titration data and changes in the O-O stretching vibration.[22] The association of Ca^{2+} (K_a = 12.2 × 10^2 ± 70 M^{-1}) can be reversed and the **^{T}P** species recovered by addition of 18-crown-6 (18-C-6). Computational models suggested side-on interaction of Ca^{2+} with the *cis*-μ-1,2-peroxido ligand as was observed in **1·Na$^+$**, but structural evidence for the Ca^{2+} adduct is so far lacking.

The identification of adduct **1·Na$^+$** raises intriguing questions about the nature of the peroxide···Na^+ interaction and how the Lewis acid affects the electronic structure as well as the spectroscopic and magnetic properties of the Cu_2O_2 core. Furthermore, trends in affinity for different alkali metal ions and the effect of these alkali metal ions on redox potentials, specifically on the oxidation of the peroxo to the superoxo species, are of interest. These questions are addressed in the present combined experimental and computational contribution.

Results and Discussion

Interaction of μ-η^1:η^1 *cis*-peroxo complex 1 with alkali metal ions in solution. Deep purple peroxo complex **1** forms upon adding dry O_2 to a colorless solution of the dicopper(I) complex $[LCu^I_2](BPh_4)$ in MeCN at -40 °C, as reported recently.[23] **1** has a characteristic UV-vis absorption spectrum showing maxima at 527 nm (ε = 5000 $M^{-1}cm^{-1}$) and 648 nm (ε = 3900 $M^{-1}cm^{-1}$) and a shoulder at 456 nm (ε = 2600 $M^{-1}cm^{-1}$). The spectrum looks similar to those of related **^{T}P** systems, whose electronic structure has been thoroughly investigated.[24,25,26] However, absorption maxima in the case of **1**, which have been assigned to $(O_2^{2-})\rightarrow Cu^{II}$ charge transfer (CT) transitions, are around two times less intense than for usual **^{T}P** complexes, reflecting a distinct bonding situation in this **^{C}P** species. This is analyzed in more detail by DFT computations, as described below.

Titrations of MeCN solutions of the alkali metal triflate salts MOTf (M^+ = Li^+, Na^+, K^+) into MeCN solutions of **1(BPh$_4$)** were monitored by UV-vis spectroscopy, revealing dramatic changes that are distinct for the different alkali metal ions but follow a clear trend (Figure 3). Upon addition of the MOTf salts, both characteristic CT bands of **1** undergo a blue shift (see Table 1) and their intensities decrease; the decrease in intensity is particularly pronounced for the lower energy absorption (assigned to $\pi^*_v\rightarrow Cu^{II}$; see below). These spectroscopic changes are reminiscent of the ones observed upon addition of $Ca(OTf)_2$ to a solution of $\{[Cu^{II}(TMPA)]_2(\mu\text{-}1,2\text{-}O_2)\}^{2+}$ in acetone (cf. Figure 2, bottom; λ_{max} = 455 nm and ε = 4080 M^{-1} cm^{-1} for the Ca^{2+} adduct of the **^{C}P** form).[22] The effect of the alkali metal ion on the optical spectrum is most dramatic for Li^+ and follows the order $Li^+ > Na^+ > K^+$. The amount of alkali metal salt required to achieve almost complete conversion to the adduct **1·M$^+$** also varies significantly, ranging from only 2 equiv. for LiOTf through ca. 10 equiv. for NaOTf to more than 50 equiv. for KOTf under the same applied conditions. Fitting the titration data using the Thordarson program[27] and a 1:1 binding model (see SI for further details) gave association constants K_a for the formation of the adducts **1·M$^+$** in MeCN that range from 62 (± 8.5%) M^{-1} for **1·K$^+$** through 65 × 10^1 (± 5.3%) M^{-1} for **1·Na$^+$** to an impressively high 69.5 × 10^4 (± 23%) M^{-1} for **1·Li$^+$** (Table 1). Addition of $[^nBu_4N]OTf$ to a solution of **1** or to dilute solutions of **1·M$^+$** did not lead to any significant changes of the respective UV–vis spectra, confirming that triflate is not directly involved in the binding equilibria. Since the Lewis acidic alkali metal ions interact with the Lewis basic peroxo unit, a decreasing strength of this interaction from Li^+ through Na^+ to K^+ can be expected in terms of the the hard and soft acids and bases (HSAB) concept[28] and in accordance with the alkali metal ion's Lewis acidity (estimated based on, e.g.,

metal-aqua pKa values or the Gutmann-Beckett method as descriptors for Lewis acidity[29]). The results are also in line with DFT computed interaction energies which are smallest for K^+ and by far largest for Li^+ (see SI, Tables S10). However, the especially strong interaction with Li^+ is surprising. Strikingly, the dicopper(II) peroxo complex **1** was found to readily abstract Li^+ from its 15-crown-5 complex, which has a quite high association constant in MeCN (10^4-10^5 M^{-1} for $[Li(15\text{-crown-}5)]^+$).[30,31]

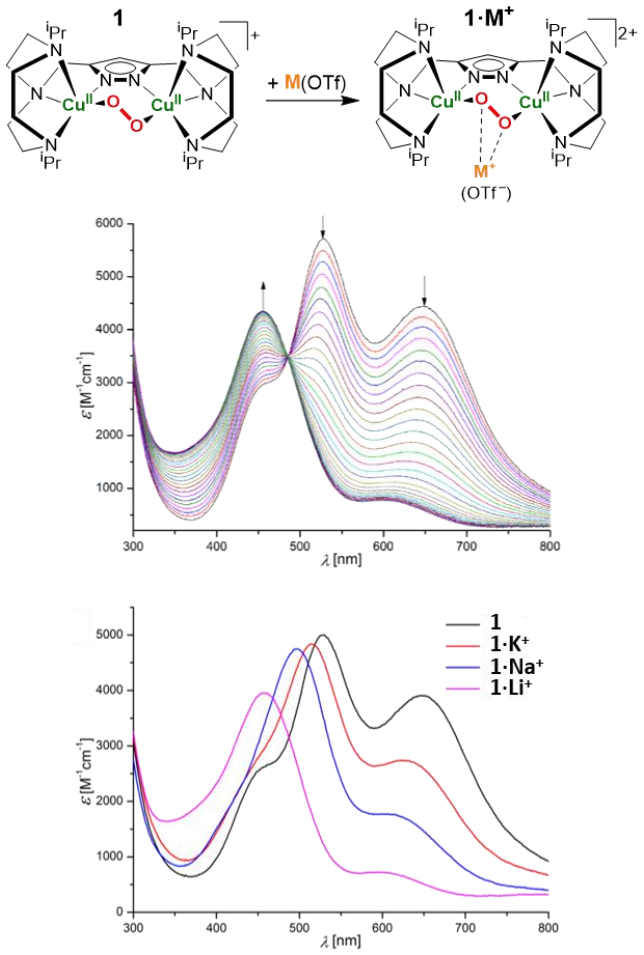

Figure 3. Top: Schematic presentation of the formation of alkali metal ion adducts **1·M⁺** upon addition of different triflate salts. Middle: UV-vis monitoring of the titration of a solution of **1** with LiOTf in steps of 0.05 equiv., with overall 2.0 equiv. added; isosbestic point at 487 nm (MeCN, T = -40 °C). Bottom: UV-vis absorption spectra (at -40 °C) of **1** and of the formed adducts **1·M⁺** after addition of the corresponding alkali metal triflate salts (**1·K⁺**: 57 equiv. KOTf; **1·Na⁺**: 15 equiv. NaOTf; **1·Li⁺**: 6 equiv. LiOTf); all complexes were prepared from the same stock solution of precursor **1** to ensure comparable conditions (for a detailed description see SI);

Table 1. Summary of association constants obtained from titration experiments of complex 2 with different alkali metal ions.

	λ_{max} [nm]	K_a [M^{-1}]
1	527, 648	-
1·K⁺	515, 624	62 (± 8.5%)
1·Na⁺	497, 612	65 × 10^1 (± 5.3%)
1·Li⁺	456, 595	69.5 × 10^4 (± 23%)

Solid state structures of adducts 1·M⁺. Following the previous report on the structural characterization of the triflate salt of **1·Na⁺**, **[1·Na(OTf)(acetone)]₂(OTf)₂**,[18] single crystalline material suitable for X-ray diffraction could now also be obtained for the triflate salts of adducts **1·Li⁺** and **1·K⁺**. Together with parent **1(BPh₄)** containing a 'naked' **^{C}P** peroxo unit,[23] this provides a unique series of four structurally characterized dicopper(II) peroxo intermediates, and allowed us to experimentally evaluate the effect of the Lewis acid interaction on metric parameters of the **^{C}P** core.

Although a large excess of KOTf is required to fully convert **1** into **1·K⁺** in MeCN solution (*vide supra*), only 1.5 equiv. of KOTf are needed to quantitatively crystallize **[1·K(OTf)(acetone)]₂(OTf)₂** from acetone/Et_2O (see SI for details). The molecular structure of the cation is depicted in Figure 4 and shows the K^+ adduct of **1** to be dimeric in the solid state, isostructural with the already reported **[1·Na(OTf)(acetone)]₂(OTf)₂**.[18] The K^+ interacts in *side-on* fashion with the peroxo unit of **1** (d(K^+···O^CO) = 2.52 Å; O^CO is the center of the peroxo O-O bond), and two **1·K⁺** entities are bridged by two triflate ions. An additional O-bound acetone molecule completes the coordination sphere of each K^+. The O-O bond length in **1·K⁺** is 1.483(4) Å, which is slightly shorter than in **1·Na⁺** (1.498(7) Å).

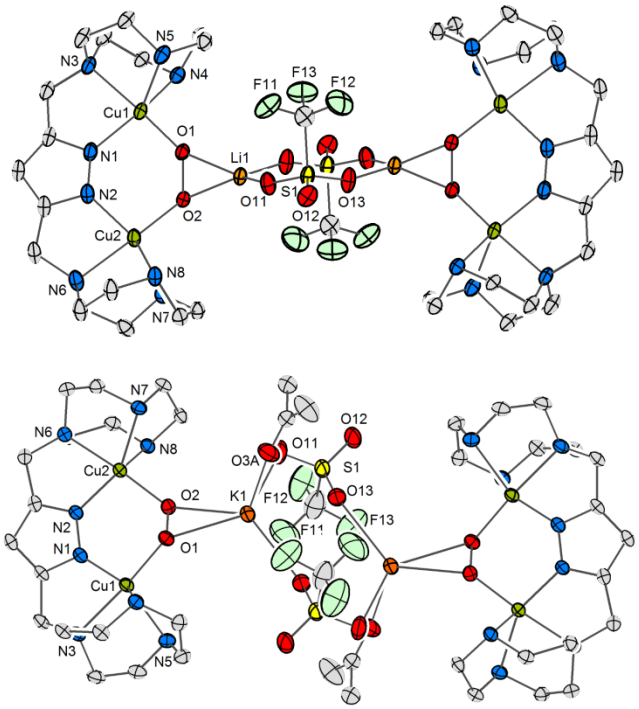

Figure 4. Solid state structures of the dimeric cations of **[1·Li(OTf)]BPh₄** (top) and **[1·K(OTf)](OTf)** (bottom), with thermal displacement ellipsoids given at 30% probability; isopropyl groups, hydrogen atoms, and counterions are omitted for clarity.

Table 2. Selected parameters of 1 and 1·M⁺ obtained from the solid state structures.[a]

	d(O-O) (Å)	*d*(O···M) (Å)[b]	*ϕ*(Cu-O-O-Cu) (°)	*d*(Cu···Cu) (Å)
1	1.441(2)	-	55.3(2)	3.7413(5)
1·K⁺	1.483(4)	2.626(3)	66.8(2)	3.7979(7)
1·Na⁺	1.498(7)	2.302(7)	65.2(5)	3.7966(12)
1·Li⁺[c]	1.497(3)	1.881(5)	71.1(2)	3.8562(9)

[a] Data for **1** and **1·Na⁺** from ref. 23 and 18, respectively

[b] The average of both M-O distances is shown here.

[c] The asymmetric unit contains two crystallographically independent monomeric cations, one of which shows a disorder in the O-O part. Values given here are from the disorder-free cation.

The adduct obtained from **1(BPh$_4$)** and LiOTf crystallizes from acetone/Et$_2$O as **[1·Li(OTf)]$_2$(BPh$_4$)$_2$** (see SI). Similarly to **1·Na⁺** and **1·K⁺**, the structure of the cation in the solid state is dimeric with two **1·Li⁺** entities spanned by two O,O′-bridging triflates. The Li⁺ is located very close to the peroxo unit (*d*(Li⁺···O^{C}O) = 1.73 Å (see remark, Table 2, footnote c)) but, because of its smaller size, it is only four-coordinate and lacks the additional acetone molecule that was found for **1·Na⁺** and **1·K⁺**. A structural comparison of parent **1** and the three adducts **1·K⁺**, **1·Na⁺** and **1·Li⁺** (Table 2) reveals a significant elongation of the peroxo O-O bond upon binding the alkali cation, which is most pronounced for **1·Na⁺** and **1·Li⁺**. Also notable is an increase in the Cu···Cu distance from around 3.74 to 3.80 Å and an increase in the Cu-O-O-Cu torsion angle from 55.3 to 71.1° in the order **1** < **1·Na⁺** < **1·K⁺** < **1·Li⁺**; the latter angle is assumed to play an important role in determining the magnetic exchange coupling between the two Cu^{II} ions (vide infra).[32] The τ_5 values[33] of the Cu^{II} ions in all adducts **1·M⁺** are in the range 0.56 – 0.58, indicating a coordination geometry in between trigonal bipyramidal and square pyramidal. In contrast, τ_5 = 0.63/0.60 for **1** reflects a distorted trigonal bipyramidal coordination sphere in the parent peroxo complex.

Computational analysis of the interaction between peroxo complex 1 and alkali metal ions. To study the interaction between the metal cation and the peroxo-dicopper(II) moiety, we performed an analysis of the charge displacement (CD) function[34,35] for the three alkali adducts (i.e. **1·M⁺**, where M⁺ = Li⁺, Na⁺, K⁺). In Figure 5b the 3D plots of the electron density difference Δρ(x,y,z) between the densities of the three adducts and those of their corresponding, non-interacting fragments are shown (see SI, section 7.1). The fragments defined here are the alkali metal cation (**M⁺**) and the [LCu$_2$O$_2$]⁺ complex (**1**). Figure 5b clearly shows that upon interaction the peroxo unit is strongly polarized toward the cation to different extents in going from **1·K⁺** to **1·Li⁺**. In particular, the large K⁺ cation is able to polarize O$_2$, but it is also mutually polarized, whereas for the adduct of the smallest and hardest alkali cation, **1·Li⁺**, a significant charge transfer from the peroxo unit to Li⁺ occurs. Figure 5a shows how much charge density is flowing leftwards, i.e. from the ligand towards Cu$_2$O$_2$, and then onwards towards the alkali metals. In order to quantitatively evaluate the net charge that has moved from the {O$_2^{2-}$} to Li⁺, we integrated Δρ across a convenient axis (see section 7.1 of the SI). At the position of the peroxo-O atoms (z = 0) the charge transfer values indicate that the lithium cation is the most acidic, with a total of 0.43e⁻ flowing in the {Cu$_2$O$_2$} → Li⁺ direction with respect to less acidic Na⁺ (CT$_{Na}$ = 0.39e⁻) and K⁺ (CT$_K$ = 0.36e⁻). These values at z = 0 are consistent with the integral of the area below the curves for z<0 that gives values of 0.45e⁻, 0.42e⁻ and 0.40e⁻ for Li⁺, Na⁺, and K⁺ respectively. This is in agreement with the Lewis acidity trend of the alkali metals, which follows the order Li⁺>Na⁺>K⁺. Interestingly, in the region between the peroxo ligand and the Cu nuclei, a significantly more pronounced charge transfer from Cu to O$_2$ is observed in the Li⁺ adduct compared to the Na⁺ and K⁺ adducts. This most likely occurs to counterbalance the electron density withdrawn from the peroxo unit by the strong Lewis acid Li⁺.

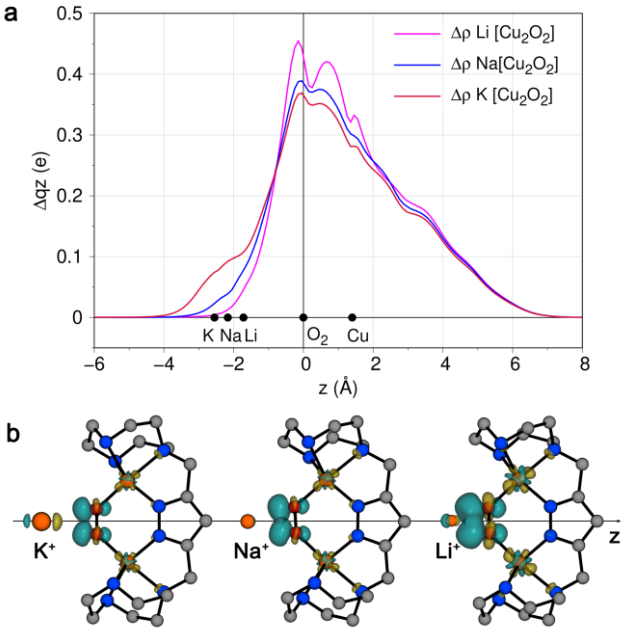

Figure 5. (a) CD curves for the complexes **1·M⁺** (M⁺ = Li⁺, Na⁺, K⁺). Black dots indicate the z position of the nuclei (K⁺, Na⁺, Li⁺; O$_2$; Cu). The vertical line at z = 0 identifies the middle of the peroxide bond (O–O) for all three complexes. (b) Isodensity surface plots (± 0.005 e$^-$ au^{-3}) of Δρ. The black arrows represent the z-axis of integration for the CD function. Yellow surfaces indicate charge depletion regions, whereas cyan surfaces identify charge accumulation regions. Isopropyl groups and hydrogen atoms are omitted for clarity.

The interaction of the alkali metal ions with the peroxo unit is evidenced by rather short M⁺···O^{C}O distances in **1·M⁺**, and thus the cations should abstract a substantial amount of electron density from the peroxide, affecting the O-O bond. Indeed, the O-O bond length changes from **1** to **1·M⁺**, but does not vary much among the three adducts. Since the solution state UV/vis absorption spectrum of **1·Li⁺** significantly deviates from those of the other complexes, the minimal structural changes upon coordination of Li⁺ are surprising. One plausible explanation would be a different geometry of the copper oxygen core in solution compared to the solid state for **1·Li⁺**, leading to different electronic structures. To investigate this possibility solid state UV/vis reflectance spectra of crystalline **1(BPh$_4$)**, **[1·K(OTf)(acetone)]$_2$(OTf)$_2$**, **[1·Na(OTf)(acetone)]$_2$(OTf)$_2$** and **[1·Li(OTf)]$_2$(BPh$_4$)$_2$** were recorded (see SI for details). However, the reflectance spectra in all cases were found to closely match the corresponding spectra of the complexes dissolved in MeCN, indicating comparable electronic structures in both the solid state and solution.

Electronic structure calculations. TD-DFT calculations allowed us to identify the molecular orbitals that account for the observed electronic transitions (Figure 6). The major transition appears red

shifted, arising from HOMO-4, the peroxide π* orbital that interacts with the Cu-centered orbitals via σ-interaction (π^*_σ), to the LUMO. The secondary transition arises from a second peroxide π* orbital (π^*_v) that is vertical to the copper oxygen plane and non-bonding. Consequently, this electronic transition occurs with lower intensity compared to the former and at lower energy.[24] The broad shoulder is due to a transition from HOMO-5, which is mainly a Cu(d_z^2) orbital.

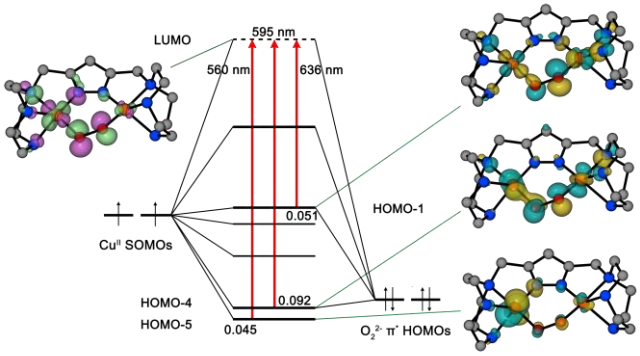

Figure 6. MO diagram derived from (ZORA)COSMO-S12g/TZ2P TD-DFT calculations. For clarity, isopropyl groups and hydrogen atoms are omitted, the $O_2(\pi^*)$ HOMO levels are shifted +3.3 eV, and only α-spin MOs are reported. Isovalue 0.04 a.u.

Upon addition of the MOTf salts and formation of adducts **1·M⁺**, both characteristic CT bands of **1** undergo a blue shift (see Table 1) and their intensities decrease; the decrease in intensity is particularly pronounced for the lower energy absorption (assigned to $\pi^*_v \rightarrow Cu^{II}$; see below). This trend is also found for the main transition in the TD-DFT calculated spectra (Figure S22 and Table S8), with a decrease in intensity for the computed secondary transition in agreement with the experimental data.

To understand better the effect of the alkali cation binding on the electronic structure of the $[LCu^{II}_2(O_2)]^+$ complex, we plotted the molecular orbitals (Figure S23-S26) as used in the TD-DFT calculation for **1** and **1·M⁺**. The $\pi^*_v(O_2)$ orbital which accounts for the secondary CT transition is the HOMO-1 in **1,** HOMO-2 in **1·K⁺** and **1·Na⁺**, and HOMO-3 in **1·Li⁺**. Conversely, the $\pi^*_\sigma(O_2)$ is always found at HOMO-4. Interestingly, as the Lewis acidity of the cation increases, the π(O_2) character of the MO decreases while the d(Cu) character is enhanced; in **1·Li⁺** the HOMO-4 symmetrized fragment orbital (SFO) population (Table S9) indicates a 53% d(Cu)-24% π(O_2) character instead of 44% d(Cu)-36% π(O_2) for **1**. Hence, in **1·Li⁺** the HOMO-4, responsible for the main CT transition, is similar to the Cu(d_z^2) HOMO-5 in **1**, which produces the broad shoulder. In other words, through the interaction with the Cu_2O_2 moiety, the alkali cation shifts the principal CT transition by modulating the π(O_2)/d(Cu) character of the molecular orbitals involved.

Effect of alkali metal ion interaction on spectroscopic and magnetic properties of *μ-η¹:η¹ cis*-peroxo complex 1. To assess the effect of alkali metal ion binding on the O-O bond, we measured resonance Raman (rR) spectra of **1** and all adducts in solution and for solid material with a laser excitation of 633 nm (see Figure 7, 8, and S3-S6). This was complemented by DFT calculations for mode assignment. As reported previously, rR spectroscopy of solid **1(BPh₄)** with λ_{exc} = 633 nm shows a pronounced band (split by Fermi resonance) for the O-O stretch at 793 cm⁻¹ that shifts to 752 cm⁻¹ when using $^{18}O_2$ ($\Delta(^{16}O_2–^{18}O_2)$ = 41 cm⁻¹, $\tilde{\nu}(^{16}O\text{-}^{16}O)$/ $\tilde{\nu}(^{18}O\text{-}^{18}O)$ = 1.055, calculated 1.060 for an isolated harmonic O-O oscillator).[23] Similar spectra with $\tilde{\nu}(^{16}O\text{-}^{16}O) \approx$ 790 cm⁻¹ ($\Delta(^{16}O_2–^{18}O_2) \approx$ 40 cm⁻¹) are observed for solid **[1·K(OTf)(acetone)]₂(OTf)₂**, **[1·Na(OTf)(acetone)]₂(OTf)₂**[18] and **[1·Li(OTf)]₂(BPh₄)₂**, though the splitting by Fermi resonance is less pronounced in the adducts; the spectrum for the Li⁺ adduct is shown in Figure 7 as an example (spectrum of the K⁺ adduct is shown in Figure S3). All O-O stretching frequencies are compiled in Table S3.

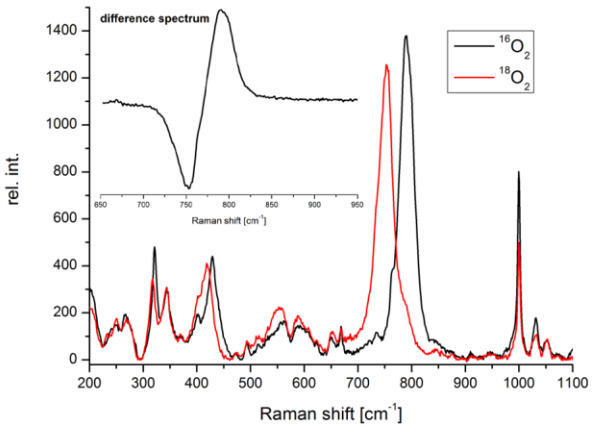

Figure 7. Resonance Raman spectra of crystalline material of **[1·Li(OTf)]₂(BPh₄)₂.**

Surprisingly, despite the significant structural changes induced by the adduct formation with alkali metal ion triflates, effects on the O-O stretching frequencies of **1** are marginal. A slight trend is obvious from the solution state experiments, which will be discussed in more detail (Figure 8). Starting from a 1×10^{-2} M solution of **1(BPh₄)** in EtCN at -30 °C, three oxygen isotope sensitive features at ca. 444, 797, and 1585 cm⁻¹ are observed. The peak at 797 cm⁻¹ (predicted at 768 cm⁻¹ by DFT, see Table S7) can be assigned to the O-O stretching vibration that appears as a doublet due to Fermi resonance (797 cm⁻¹ is the average shift of the doublet), and collapses into a single band upon labeling with $^{18}O_2$ ($\Delta(^{16}O_2–^{18}O_2)$ = 39 cm⁻¹ (exp), 35 cm⁻¹ (DFT)); this phenomenon has also been reported for many other **ᵀP** systems.[32,36,37] In the presence of the Lewis acids, the O-O stretch shifts slightly to lower energies (796 cm⁻¹ for **1·K⁺**, 791 cm⁻¹ for **1·Li⁺**; see Table S3), in accordance with the elongation of the O-O bond found in the molecular structures (see Table 2). The second oxygen-isotope-sensitive feature at 1585 cm⁻¹ can be assigned to the overtone of the O-O stretching vibration and hence also shifts to lower wavenumbers in the presence of an alkali metal ion (1576 cm⁻¹ for **1·K⁺**, 1571 cm⁻¹ for **1·Na⁺**). However, this shift is more pronounced compared to the normal mode, suggesting increased anharmonicity in the adducts. These bands above 1550 cm⁻¹ are not observed in the DFT calculated spectra, corroborating their overtone character (not observable within the harmonic approximation used in DFT[38]). A further oxygen-sensitive feature at ca. 444 cm⁻¹ (DFT: 427 cm⁻¹, $\Delta^{18}O_2$ = 19 cm⁻¹ (exp), 29 cm⁻¹ (DFT)) can be assigned to a Cu-O stretch that is only poorly resolved in the experiments, while rather appreciable from DFT calculations. In all cases, a shift to higher energies is observed when the alkali metals are present. Besides these oxygen sensitive stretches, other resonance-enhanced Raman features at ca. 270, ca. 330 and at ca. 350 cm⁻¹ can be observed. These signals presumably correspond to Cu-N stretches of the central pyrazolato unit and of the TACN sides arms.[37]

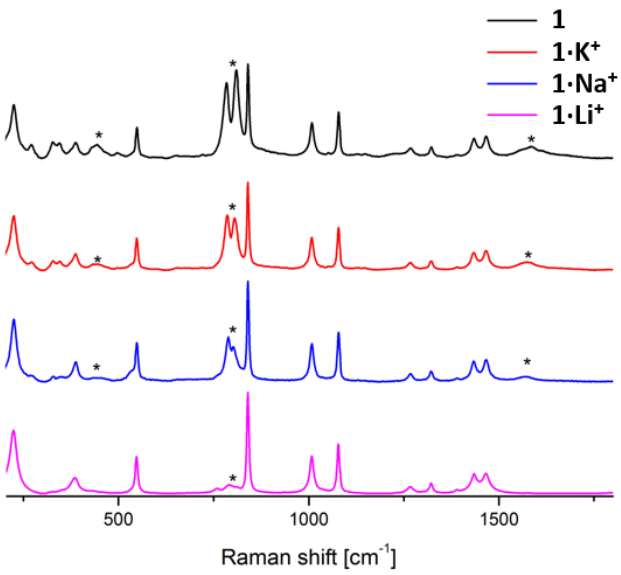

Figure 8. Resonance Raman spectra of **1** and adducts **1·M⁺** in EtCN at -30 °C (c = 1 × 10-2 M, λ_{exc} = 633 nm). ^{18}O-sensitive signals are labeled (*). Spectra have been scaled relative to the solvent signals.

While the energies of the O-O stretch are not significantly affected upon interaction with the alkali metal ions, the O-O vibration is clearly losing intensity when going from **1** to **1·Li⁺** (see Figure 8**)**. Consequently, the overtone as well as the Cu-O stretch, which are already poorly resolved in **1**, vanish in the spectrum of **1·Li⁺** (note that rR spectra shown in Figure 8 have been recorded under the same conditions and spectra have been scaled relative to the solvent signals). The drastic loss of intensity upon adduct formation may be explained by considering the UV-vis absorption spectra of the different peroxo complexes, along with the schematic MO diagram of **1** (see Figure 6 and Figures S23-S26). Upon adduct formation a shift of the absorption maxima of all adducts to higher energies is observed concomitant with a decrease of their intensities, when the rR excitation wavelength is retained at 633 nm. With respect to a distortion of the O-O bond that is resonance enhanced during this experiment, a $\pi^*_v(O_2^{2-})$ to copper CT transition is believed to have a greater effect on the O-O bond than a transition from the $\pi^*_\sigma(O_2^{2-})$ orbital, which has less electron density with antibonding character within the peroxo region.[24] Consequently, the changes in intensity of the oxygen-sensitive features in the resonance-enhanced Raman spectra arise from a drastic loss of intensity of the $\pi^*_v(O_2^{2-})$-to-copper CT transition upon alkali metal binding, which is simultaneously shifting out of the excitation wavelength of 633 nm.

The shift of the O-O stretching frequency towards lower wavenumbers, though only minor, is in line with the observed increase in O-O bond lengths upon M^+ binding (see Table 2). However, when considering solely the interaction of the peroxide group with the Lewis acidic alkali metal ions, the trend is counterintuitive because this M-O_2 interaction should lead to removal of electron density from the antibonding peroxo π* orbitals, thus stabilizing the O-O bond. Nevertheless, this removal of electron density is compensated by the transfer of charge density from Cu and its N-donor ligands towards the peroxo (see Figure 5a), in particular for **1·Li⁺**. Both charge-flows directly influence the frontier MOs, with both the HOMO and LUMO showing larger contributions from copper d-orbitals upon binding of the alkali metals (see Table S9). In contrast, the peroxo contributes more to lower-lying orbitals (such as HOMO-3 and HOMO-5). Overall, the contribution of the oxygen p-orbitals to the MOs increases gradually, from 449% (out of a maximum of 600% if the three p-orbitals of both oxygens were fully occupied) for **1**, to 456% for **1·K⁺**, 457% for **1·Na⁺** and 458% for **1·Li⁺**. This is qualitatively consistent with the trend in O-O bond lengths, which become longer, i.e., reflecting a larger contribution of the antibonding peroxo π* orbitals. The gradual increase of the Cu-O distances from 1.894 Å in **1**, to 1.900 Å in **1·Na⁺**, 1.908 Å in **1·Na⁺** and 1.909 Å in **1·Li⁺** indicate a weakening of the Cu-O bonds. Both the weakened O-O and Cu-O bonds and the shifts in the contributions of the frontier MOs can explain the loss of intensity of the CT transitions upon alkali metal binding. In particular, the second CT transition (648 nm for **1**) is affected by the changes in MO compositions; this transition corresponds to the $\pi^*_v(O_2^{2-})\rightarrow Cu^{II}$ charge transfer in all cases, originating (mainly) from HOMO-1 for **1**, HOMO-2 for **1·K⁺** and **1·Na⁺**, and HOMO-3 for **1·Li⁺**. The increased energetic separation between these occupied MOs and the receiving LUMO, as well as the smaller overlap between the two, makes the transition less efficient, leading to larger excitation energies (lower wavelengths) and reduced oscillator strengths (intensities). Thus, in going from **1** to the adducts **1·M⁺**, more electron density with antibonding character is observed within the peroxo region, which progressively destabilizes the O-O bond, and reduces the CT transitions at the same time.

Magnetic properties of the *μ-η¹:η¹ cis*-peroxo complexes. As was previously demonstrated, the Cu-O-O-Cu dihedral angle ϕ in μ-η¹:η¹-peroxodicopper(II) complexes has a dramatic effect on the magnetic coupling and the spin ground state.[32] Though experimental data are scarce, known **ᵀP** complexes with $\phi \approx 180°$ usually have a strongly stabilized S = 0 ground state due to antiferromagnetic coupling between the two Cu^{II} (S = ½) ions with $-2J > 600$ cm^{-1} ($\hat{H} = -2J\hat{S}_1\hat{S}_2$).[39] The same situation is expected for an ideal **ᶜP** system with $\phi \approx 0°$, but in case of the first **ᶜP** type complex **[1·Na(OTf)(acetone)]₂(OTf)₂** with a Cu-O-O-Cu dihedral angle of 65.2° the antiferromagnetic coupling was found to be much attenuated, viz. $-2J$ = 154 cm^{-1}.[18] A related pyrazolate-based μ-η¹:η¹-peroxodicopper(II) complex with a Cu-O-O-Cu torsion close to 90° (ϕ = 104.2°), which is best described as a **⊥P** system right in between **ᵀP** and **ᶜP** (Figure 2), showed rather strong ferromagnetic coupling ($-2J$ = −144 cm^{-1}) attributed to orthogonality of the magnetic orbitals (e.g., Cu($d_{x^2-y^2}$) for an ideal square pyramidal geometry), and a vanishing overlap integral of these orbitals through the bridging peroxide ligand.[32]

The magnetic properties of solid samples of parent **1(BPh₄)** as well as of the new adducts **[1·K(OTf)(acetone)]₂(OTf)₂** and **[1·Li(OTf)]₂(BPh₄)₂** have now been studied by SQUID magnetometry. The temperature dependence of the molar magnetic susceptibility χ_M for **1** and for all three adducts is shown in Figure 9. The difference in the magnetic behavior is evident from the position of the maxima in the χ_M vs T plots (T_{max}), since T_{max} is linearly correlated with the exchange coupling constant J, i.e. the stronger the coupling the higher the temperature where the maximum is observed (in this notation, Boltzmann constant k_B = 0.695 cm^{-1}K^{-1}).[40] Values for $-2J$ obtained from best fits of the magnetic data (for details see SI) are given in Table 3, together with key metric parameters. In **[1·K(OTf)(acetone)]₂(OTf)₂** the Cu-O-O-Cu torsion angle is very similar to the one in **[1·Na(OTf)(acetone)]₂(OTf)₂** (66.8° vs. 65.2°), and the singlet-triplet splitting is found to be the same ($-2J$ = 154 cm^{-1}). In contrast, the Cu-O-O-Cu torsion increases to 71° in **[1·Li(OTf)]₂(BPh₄)₂** while antiferromagnetic coupling of the

Cu^{II} ions centers is significantly diminished ($-2J$ = 80 cm^{-1}), in accordance with the qualitative considerations outlined above. Parent *μ-η¹:η¹* peroxo complex **1(BPh₄)**, however, shows a rather small singlet-triplet splitting of $-2J$ = 111 cm^{-1} despite having the smallest Cu-O-O-Cu torsion angle within the series, ϕ = 55°. One possible explanation may be the different coordination environments of the Cu^{II} ions in **1** compared to the adducts **1·M⁺**. Whereas the average τ_5 values ($\bar{\tau}_5$) of both Cu^{II} ions in the three adducts **1·M⁺** are similar (Table 3), $\bar{\tau}_5$ in **1** indicates a major distortion towards a trigonal bipyramidal geometry. This results in a different character of the Cu-centered magnetic orbitals and a potentially decreased overlap of ligand and metal orbitals, consequently diminishing the amount of magnetic exchange.[41,42] It should also be noted that the two Cu^{II} ions will couple magnetically via both the peroxide and the pyrazolate bridges. Here, contributions from the peroxide mediated exchange pathways are assumed to be predominant since dinuclear Cu^{II} complexes with a single pyrazolate as the only bridging unit typically show weak magnetic coupling ($-2J$ = 30-70 cm^{-1}).[43,44] However, contributions of the pyrazolate bridge to the overall magnetic interaction in ions in **1** and **1·M⁺** will not be negligible. These findings illustrate that the interplay of multiple factors such as the Cu-O-O-Cu torsion angle and the Cu-N-N-Cu fragment, as well as the coordination environment of the Cu^{II} ions, will affect the magnitude of magnetic exchange coupling in these pyrazolate-based *μ-η¹:η¹* peroxodicopper(II) complexes.

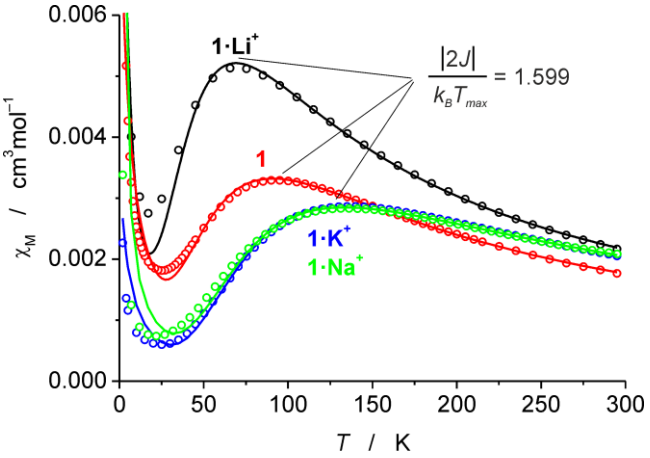

Figure 9. Temperature dependence of χ_M of **1** and the three adduct complexes **1·M⁺**; the solid curves show the best fits obtained.

Table 3. Cu-O-O-Cu torsion angles, average $\bar{\tau}_5$ values and magnetic coupling constants of 1 and 1·M⁺.

	ϕ Cu-O-O-Cu [°]	($\bar{\tau}_5$)	$-2J$ [cm^{-1}]
1	55.3(2)	0.62	111
1·K⁺	66.8(2)	0.56	154
1·Na⁺	65.2(5)	0.58	154
1·Li⁺[a]	71.1(2)	0.56	80

[a] The asymmetric unit contains two crystallographically independent monomeric cations, one of which shows a disorder in the O-O part. The value given here is from the disorder-free cation.

Spin state splitting DFT calculations, carried out on the crystal coordinates of **1** and **1·M⁺** (Table S11) show reasonably good agreement with small singlet-triplet splittings (considering the expected accuracy for these calculations which is of the order of 1-2 kcal·mol^{-1}, i.e. 350-700 cm^{-1}). The OPBE functional correctly predicts the singlet ground state of all three adducts **1·M⁺**, although for parent **1** the triplet is incorrectly lower in energy. However, it is worth noting that the spin state splitting of **1** using OPBE is the closest to the experimental value among all the DFT functionals tested in this work (see SI).

Effect of alkali ion interaction on electrochemical properties of *μ-η¹:η¹ cis*-peroxo complex 1. As reported recently, parent *cis*-μ-η¹:η¹-peroxo complex **1** can be reversibly oxidized to the corresponding μ-η¹:η¹-superoxo complex $[LCu^{II}_2(O_2)]^{2+}$ (**2**) at low potential (–0.58 V vs. Fc/Fc^+; Figure 10), followed by an irreversible further oxidation at ca. 0.6 V, likely associated with the liberation of O_2 (see Figure S19).[23]

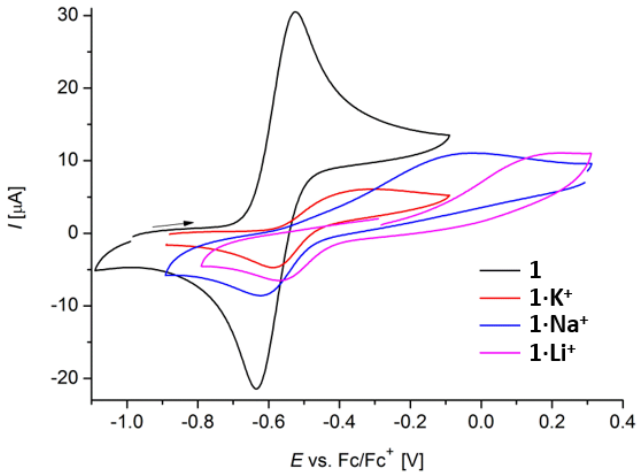

Figure 10. Cyclic voltammograms showing first oxidation of complex **1** (black) and its alkali metal ion adducts **1·M⁺** recorded at 100 mV/s scan rate and 0 °C (MeCN/0.1 M $^nBu_4NPF_6$); final concentrations for **1**: 3.02 mM; **1·K⁺**: 2.67 mM; **1·Na⁺**: 2.26 mM; **1·Li⁺**: 2.69 mM.

For a preliminary assessment of the effect of the Lewis acidic alkali metal ions on the electrochemical properties of **1**, adducts **1·M⁺** were prepared in situ by adding concentrated solutions of the corresponding alkali metal triflate salt M(OTf) to preformed **1** in MeCN/0.1 M $^nBu_4NPF_6$ until no further change of the cyclic voltammograms (CVs) was observed; under these conditions complete formation of adducts **1·M⁺** is assumed (required excess of MOTf for **1·Li⁺**: 19 equiv.; **1·Na⁺**: 39 equiv.; **1·K⁺**: 119 equiv.). The resulting CV traces for the first oxidation are shown in Figure 10. In the presence of alkali cations, the anodic peak potential E^1_{pa} shifts strongly towards higher potential, the CV waves become broad, and the redox process loses electrochemical reversibility. The total shift of E^1_{pa} increases from **1·K⁺** to **1·Li⁺**, which reflects the interaction strength of the Lewis acid with the peroxo unit and the corresponding charge flow from the $\{O_2^{2-}\}$ to M^+ (cf. Figure 5). Interestingly, the shift of E^1_{pa} appears to correlate linearly with the Lewis acidity of the metal ions M^+ (Figure S20). Titration experiments with MOTf show that the dicationic superoxo complex does not interact with the alkali metal ions. Therefore oxidation of **1·M⁺** induces dissociation of M^+ from the resulting Cu^{II}-$O_2^{\bullet-}$-Cu^{II} core. As such the peak potential of the second anodic process associated with oxidation of the superoxo unit, E^2_{pa}, as well as the cathodic

peak potential E_{pc} in the reverse scan are both much less affected by the presence of M^+ and are barely shifted compared to parent **1** (Figures 10 and S19)

Conclusions

Increasing evidence suggests that the properties and reactivities of metal-dioxygen intermediates are strongly influenced by interaction with redox-inactive Lewis acidic metal ions, but structural insight for such adducts has so far been extremely scarce. In this work we have now isolated and fully analyzed an entire alkali metal series of a *cis*-μ-η^1:η^1-peroxo dicopper(II) complex (**1**), which also provides several crystallographically characterized examples for this rare ^{c}**P** type Cu_2O_2 binding motif. Li^+, Na^+ and K^+ are found *side-on* bound to the peroxo unit, leading to a significant O-O bond elongation compared to parent **1**, yet effects on the O-O stretching frequencies are minor. The strength of interaction in MeCN solution has been quantified and is found to vary considerably for the different alkali metal cations, with a remarkably high affinity for Li^+ which is even extracted from its crown ether complex. Interaction of Li^+, Na^+ and K^+ is evidenced by drastic changes observed in the UV-vis spectra of the different adducts, which are consistent in both solution and in the solid state. Computational analysis across the series shows pronounced differences in the degree of charge transfer from copper to the O_2 fragment, indicating that the entire Cu-OO-Cu unit is affected. This also explains the significant differences in optical properties, because the alkali cation shifts the principal CT transition by modulating the $\pi(O_2)$/d(Cu) character of the molecular orbitals involved. In addition, association with the various alkali metal cations leads to variations in the Cu-O-O-Cu torsion angle, which has a sizeable effect on the strength of antiferromagnetic coupling between the two Cu^{II} ions, allowing us to establish a qualitative magneto-structural correlation for the ^{c}**P** motif. The modulation of the dicopper-peroxo unit further extends to the electrochemical properties of the complexes, where a substantial shift of the anodic peak potential and a loss of electrochemical reversibility for the peroxo/superoxo interconversion are observed in the presence of alkali metal ions.

While previous studies on the effects of redox-inactive Lewis acids on metal/dioxygen intermediates have mostly employed strongly Lewis acidic di- and trivalent metal ions such as Ca^{2+} or Sc^{3+}, the present study shows that even monocationic and relatively weakly Lewis acidic alkali metal ions can lead to significant changes in electronic structures and spectroscopic signatures. These findings also suggest that much care must be taken when reporting characteristics of reactive intermediates prepared in situ, as alkali metal ions, which are often present in the reaction mixtures (e.g., from the use of alkali metal ion containing bases or other reagents) but are usually thought to be innocent 'spectators', can indeed play a direct role and have a profound influence on electronic, magnetic and electrochemical properties. These interactions, which have been structurally authenticated and quantitatively assessed for the present ^{c}**P** type Cu_2O_2 intermediates, are also reminiscent of those exerted by polarizing residues and ions present in enzyme active sites, and they warrant further attention given the ubiquity of alkali metal ions in both nature and the laboratory.

Experimental Section

See supporting information for experimental details and instrumentation.

Associated Content

Supporting information

Synthesis of shown complexes and their crystallographic details, UV/vis titration experiments, solid state UV/vis spectra, rR spectra in solution and in the solid state, SQUID data of all complexes and DFT calculations. This material is available free of charge via the Internet at http://pubs.acs.org

Author Information

Corresponding authors

*E-mail: Franc.Meyer@chemie.uni-goettingen.de
*E-mail: Marcel.Swart@gmail.com

ORCID

Lorenzo D'Amore: 0000-0003-2245-1956
Sebastian Dechert: 0000-0002-2864-2449
Marcel Swart: 0000-0002-8174-8488
Franc Meyer: 0000-0002-8613-7862

Notes

The authors declare no competing financial interest

Acknowledgement

This work was performed in the framework of the European COST action CM1305 (ECOSTBio). It was supported by the Deutsche Forschungsgemeinschaft (PhD scholarship for Alexander Brinkmeier within the IRTG 1422 "Metal sites in Biomolecules: Structures, Regulation and Mechanisms"), the Ministerio de Economia y Competitividad (MINECO, projects CTQ2014-59212-P, CTQ2015-70851-ERC and CTQ2017-87392-P), the DIUE of the Generalitat de Catalunya (project 2014SGR1202), the European Fund for Regional Development (FEDER, UNGI10-4E-801) and Universitat de Girona (scholarship for Lorenzo D'Amore).

References

(1) Zhang, X.-P.; Chandra, A.; Lee, Y.-M.; Cao, R.; Ray, K.; Nam, W. Transition metal-mediated O–O bond formation and activation in chemistry and biology. *Chem. Soc. Rev*. **2021**, *50*, 4804–4811.

(2) Liu Y.; Lau T.-C. Activation of Metal Oxo and Nitrido Complexes by Lewis Acids. *J. Am. Chem. Soc.* **2019**, *141*, 3755−3766.

(3) Devi, T.; Lee, Y.-M.; Nam, W.; Fukuzumi, S. Metal ion-coupled electron-transfer reactions of metal-oxygen complexes. *Coord. Chem. Rev.* **2020**, *410*, 213219.

(4) Yano, J.; Yachandra, V. Mn_4Ca Cluster in Photosynthesis: Where and How Water is Oxidized to Dioxygen. *Chem. Rev.* **2014**, 114, 4175−4205.

(5) (a) Pfaff, F. F.; Kundu, S.; Risch, M.; Pandian, S.; Heims, F.; Pryjomska-Ray, I.; Haack, P.; Metzinger, R.; Bill, E.; Dau, H.; Comba, P.; Ray, K. An Oxocobalt(IV) Complex Stabilized by Lewis Acid Interactions with Scandium(III) Ions. *Angew. Chem. Int. Ed.* **2011**, *50*, 1711–1715; (b) Hong, S.; Pfaff, F. F.; Kwon, E.; Wang, Y.; Seo, M.-S.; Bill, E.; Ray, K.; Nam, W. Spectroscopic Capture and Reactivity of a Low-Spin Cobalt(IV)-Oxo Complex Stabilized by Binding Redox-Inactive Metal Ions. *Angew. Chem. Int. Ed.* **2014**, *53*, 10403–10407.

(6) (a) Leeladee, P.; Baglia, R. A.; Prokop, K. A.; Latifi, R.; de Visser, S. P.; Goldberg, D. P. Valence Tautomerism

in a High-Valent Manganese–Oxo Porphyrinoid Complex Induced by a Lewis Acid. *J. Am. Chem. Soc.* **2012**, *134*, 10397–10400; (b) Baglia, R. A.; Dürr, M.; Ivanovic-Burmazović, I.; Goldberg, D. P. Activation of a High-Valent Manganese–Oxo Complex by a Nonmetallic Lewis Acid. *Inorg. Chem.* **2014**, *53*, 5893–5895.

(7) Fukuzumi, S.; Ohkubo, K.; Lee, Y.-M.; Nam, W. Lewis Acid Coupled Electron Transfer of Metal–Oxygen Intermediates. *Chem. Eur. J.* **2015**, *21*, 17548 – 17559.

(8) Kim, K.; Cho, D.; Noh, H.; Ohta, T.; Baik, M.-H.; Cho, J. Controlled Regulation of the Nitrile Activation of a Peroxocobalt(III) Complex with Redox-Inactive Lewis Acidic Metals. *J. Am. Chem. Soc.* **2021**, *143*, 11382-11392.

(9) Fukuzumi, S.; Morimoto, Y.; Kotani, H.; Naumov, P., Lee, Y.-M.; Nam, W. Crystal structure of a metal ion-bound oxoiron(IV) complex and implications for biological electron transfer. *Nature Chem.* **2010**, *2*, 756–759.

(10) (a) Swart, M. A change in the oxidation state of iron: scandium is not innocent. *Chem. Commun.* **2013**, *49*, 6650–6652; (b) Prakash, J.; Rohde, G. T.; Meier, K. K.; Jasniewski, A. J.; Van Heuvelen, K. M.; Münck, E.; Que Jr., L. Spectroscopic Identification of an Fe^{III} Center, not Fe^{IV}, in the Crystalline Sc–O–Fe Adduct Derived from $[Fe^{IV}(O)(TMC)]^{2+}$. *J. Am. Chem. Soc.* **2015**, *137*, 3478–3481.

(11) (a) Lee, Y.-M.; Bang, S.; Kim, Y. M.; Cho, J.; Hong, S.; Nomura, T.; Ogura, T.; Troeppner, O.; Ivanović-Burmazović, I.; Sarangi, Ri.; Fukuzumi, S.; Nam, W. A mononuclear nonheme iron(III)–peroxo complex binding redox-inactive metal ions. *Chem. Sci.* **2013**, *4*, 3917–3923; (b) Bang, S.; Lee, Y.-M.; Hong, S.; Cho, K.-B.; Nishida, Y.; Seo, M. S.; Sarangi, R.; Fukuzumi, S.; Nam, W. Redox-inactive metal ions modulate the reactivity and oxygen release of mononuclear non-haem iron(III)–peroxo complexes. *Nature Chem.* **2014**, *6*, 934-940.

(12) Bae, S. H.; Lee, Y.-M.; Fukuzumi, S.; Nam, W. Fine Control of the Redox Reactivity of a Nonheme Iron(III)–Peroxo Complex by Binding Redox-Inactive Metal Ions. *Angew. Chem. Int. Ed.* **2017**, *56*, 801 –805.

(13) Li, F.; Van Heuvelen, K. M.; Meier, K. K., Münck, E.; Que Jr., L. Sc^{3+}-Triggered Oxoiron(IV) Formation from O_2 and its Non-Heme Iron(II) Precursor via a Sc^{3+}–Peroxo–Fe^{3+} Intermediate. *J. Am. Chem. Soc.* **2013**, *135*, 10198–10201.

(14) Banerjee, S.; Draksharapu, A.; Crossland, P. M.; Fan, R.; Guo, Y.; Swart, M.; Que Jr., L. Sc^{3+}-Promoted O–O Bond Cleavage of a (μ-1,2-Peroxo)diiron(III) Species Formed from an Iron(II) Precursor and O_2 to Generate a Complex with an $Fe^{IV}_2(\mu\text{-}O)_2$ Core. *J. Am. Chem. Soc.* **2020**, *142*, 4285–4297.

(15) Garcia-Bosch, I.; Cowley, R. E.; Díaz, D. E.; Peterson, R. L.; Solomon, E. I.; Karlin, K. D. Substrate and Lewis Acid Coordination Promote O–O Bond Cleavage of an Unreactive $L_2Cu^{II}_2(O_2^{2-})$ Species to Form $L_2Cu^{III}_2(O)_2$ Cores with Enhanced Oxidative Reactivity. *J. Am. Chem. Soc.* **2017**, *139*, 3186–3195.

(16) Kakuda, S.; Rolle, C. J.; Ohkubo, K.; Siegler, M. A.; Karlin, K. D.; Fukuzumi, S. Lewis Acid-Induced Change from Four- to Two-Electron Reduction of Dioxygen Catalyzed by Copper Complexes Using Scandium Triflate. *J. Am. Chem. Soc.* **2015**, *137*, 3330–3337.

(17) (a) Schax, F.; Suhr, S.; Bill, E.; Braun, B.; Herwig, C.; Limberg, C. A Heterobimetallic Superoxide Complex formed through O_2 Activation between Chromium(II) and a Lithium Cation. *Angew. Chem. Int. Ed.* **2015**, *54*, 1352 –1356; (b) Wind, M.-L.; Hoof, S.; Herwig, C.; Braun-Cula, B.; Limberg, C. The Influence of Alkali Metal Ions on the Stability and Reactivity of Chromium(III) Superoxide Moieties Spanned by Siloxide Ligands. *Chem. Eur. J.* **2019**, *25*, 5743 – 5750.

(18) Dalle, K. E.; Gruene, T.; Dechert, S.; Demeshko, S.; Meyer, F. Weakly Coupled Biologically Relevant $Cu^{II}_2(\mu\text{-}\eta^1\text{:}\eta^1\text{-}O_2)$ *cis*-Peroxo Adduct that Binds Side-On to Additional Metal Ions. *J. Am. Chem. Soc.* **2014**, *136* , 7428 - 7434.

(19) Elwell, C. E.; Gagnon, N. L.; Neisen, B. D.; Dhar, D.; Spaeth, A. D.; Yee, G. M.; Tolman, W. B. Copper–Oxygen Complexes Revisited: Structures, Spectroscopy, and Reactivity. *Chem. Rev.* **2017**, *117*, 2059-2107.

(20) Solomon, E. I.; Chen, P.; Metz, M.; Lee, S.-K.; Palmer, A. E. Oxygen Binding, Activation, and Reduction to Water by Copper Proteins. *Angew. Chemie Int. Ed.* **2001**, *40*, 4570 - 4590.

(21) Metz, M.; Solomon, E. I. Dioxygen Binding to Deoxyhemocyanin: Electronic Structure and Mechanism of the Spin-Forbidden Two-Electron Reduction of O_2. *J. Am. Chem. Soc.* **2001**, *123*, 4938 - 4950.

(22) Vargo, N. P.; Harland, J. B.; Musselman, B. W.; Lehnert, N.; Ertem, M. Z.; Robinson, J. R. Calcium-Ion Binding Mediates the Reversible Interconversion of Cis and Trans Peroxido Dicopper Cores. *Angew. Chem. Int. Ed.* **2021**, *60*, 19836-19842.

(23) Brinkmeier, A.; Schulz, R. A.; Buchhorn, M.; Spyra, C.-J.; Dechert, S.; Demeshko, S.; Krewald, V.; Meyer, F. Structurally Characterized μ-1,2-Peroxo/Superoxo Dicopper(II) Pair. *J. Am. Chem. Soc.* **2021**, *143*, 10361-10366.

(24) Baldwin, M. J.; Ross, P. K.; Pate, J. E.; Tyeklar, Z.; Karlin, K. D.; Solomon, E. I. Spectroscopic and Theoretical Studies of an End-On Peroxide-Bridged Coupled Binuclear Copper(II) Model Complex of Relevance to the Active Sites in Hemocyanin and Tyrosinase. *J. Am. Chem. Soc.* **1991**, *113*, 8671-8679.

(25) Solomon, E. I.; Baldwin, M. J.; Lowery, M. D. Electronic Structures of Active Sites in Copper Proteins: Contributions to Reactivity. *Chem. Rev.* **1992**, *92*, 521-542.

(26) Mirica, L. M.; Ottenwaelder, X.; Stack, T. D. P. Structure and Spectroscopy of Copper–Dioxygen Complexes. *Chem. Rev.* **2004**, *104*, 1013-1046.

(27) Thordarson, P. *Chem. Soc. Rev.* **2011**, *40*, 1305-1323.

(28) Pearson, R. G. J. Hard and Soft Acids and Bases. *J. Am. Chem. Soc.* **1963**, *85*, 3533 - 3539.

(29) Kumar, A.; Blakemore, A. D. On the Use of Aqueous Metal-Aqua pK_a Values as a Descriptor of Lewis Acidity. *Inorg. Chem.* **2021**, *60*, 1107–1115.

(30) Cahen, Y. M.; Dye, J. L.; Popov, A. I. Lithium-7 Nuclear

Magnetic Resonance Study of Lithium Ion-Lithium Cryptate Exchange Rates in Various Solvents. *J. Phys. Chem.* **1975**, *79*, 1292 - 1295.

(31) Takeda, Y.; Katsuta, K.; Inoue, Y.; Hakushi, T. Bull. A Conductance Study of 1:1 Complexes of 15-Corwn-5, 16-Crown-5, and Benzo-15-crown-5 with Alkali Metal Ions in Nonaqueous Solents. *Chem. Soc. Jpn.* **1988**, 627–632.

(32) Kindermann, N.; Bill, E.; Dechert, S.; Demeshko, S.; Reijerse, E. J.; Meyer, F. A Ferromagnetically Coupled (S = 1) Peroxodicopper(II) Complex. *Angew. Chem. Int. Ed.* **2015**, *54*, 1738-1743.

(33) Addison, A. W.; Rao, T. N.; Reedijk, J.; Van Rijn, J.; Verschoor, G. C. Synthesis, structure, and spectroscopic properties of copper(II) compounds containing nitrogen-sulfur donor ligands: the crystal and molecular structure of aqua[1,7-bis(N-methylbenzimidazol-2'-yl)-2,6-dithiaheptane] copper(II) perchlorate. *J. Chem. Soc., Dalton Trans.* **1984**, *7*, 1349-1356.

(34) Belpassi, L.; Infante, I.; Tarantelli, F.; Visscher, L. The Chemical Bond between Au(I) and the Noble Gases. Comparative Study of NgAuF and $NgAu^+$ (Ng = Ar, Kr, Xe) by Density Functional and Coupled Cluster Methods. *J. Am. Chem. Soc.* **2008**, *130*, 1048-1060.

(35) D'Amore, L.; Belpassi, L.; Klein, J.E.M.N.; Swart, M. Spin-resolved charge displacement analysis as an intuitive tool for the evaluation of cPCET and HAT scenarios. *Chem. Commun.* **2020**, *56*, 12146-12149.

(36) Peterson, R. L.; Himes, R. A.; Kotani, H.; Suenobu, T.; Tian, L.; Siegler, M. A.; Solomon, E. I.; Fukuzumi, S.; Karlin, K. D. Cupric Superoxo-Mediated Intermolecular C-H Activation Chemistry. *J. Am. Chem. Soc.* **2011**, *133*, 1702-1705.

(37) Henson, M. J.; Vance, M. A.; Zhang, C. X.; Liang, H.; Karlin, K. D.; Solomon, E. I. Resonance Raman Investigation of Equatorial Ligand Donor Effects on the $Cu_2O_2^{2+}$ Core in End-On and Side-On μ-Peroxo-Dicopper(II) and Bis-μ-oxo-Dicopper(III) Complexes. *J. Am. Chem. Soc.* **2003**, *125*, 5186 - 5192.

(38) Brauer, B.; Dubnikova, F.; Zeiri, Y.; Kosloff, R,: Gerber, R. B. Vibrational spectroscopy of tracetone triperoxide (TATP): Anharmonic fundamentals, overtones and combination bands. *Spectrochimica Acta* **2008**, *71*, 1438 - 1445.

(39) Karlin, K. D.; Tyeklár, Z.; Farooq, A.; Jacobson, R. R.; Sinn, E.; Lee, D. W.; Bradshaw, J. E.; Wilson, L. J. Peroxide (O_2^{2-}) as a bridging ligand for copper(II): strong exchange coupling in complexes derived from copper(I) and dioxygen. *Inorg. Chim. Acta* **1991**, *182*, 1–3.

(40) O. Kahn, *Molecular Magnetism*, VCH Publishers Inc., New York, **1993**.

(41) Matsushima, H.; Hamada, H.; Watanabe, K.; Koikawa, M.; Tokii, T. Magnetic properties and crystal structures of bis(μ-pyrazolato)-bridged dicopper(II,II) complexes with 1,10-phenanthroline or 2,2'-bipyridine. *J. Chem. Soc. Dalt. Trans.* **1999**, 971-977.

(42) Singh, A. K.; Vlugt, I. Van Der; Demeshko, S.; Dechert, S.; Meyer, F. Bis(terdentate) Pyrazole/Pyridine Ligands: Synthesis, Crystal Structures and Magnetic Properties of Bridged Binuclear and Tetranuclear Copper(II) Complexes. *Eur. J. Inorg. Chem.* **2009**, 3431-3439.

(43) Prokofieva, A.; Prikhod'ko, A. I.; Enyedy, E. A.; Farkas, E.; Maringgele, W.; Demeshko, S.; Dechert, S.; Meyer, F. Oligonuclear Copper Complexes of a Bioinspired Pyrazolate-Bridging Ligand: Synthesis, Structures, and Equilibria in Solution. *Inorg. Chem.* **2007**, *46*, 4298-4307.

(44) Driessen, W. L.; Chang, L.; Finazzo, C.; Gorter, S.; Rehorst, D.; Reedijk, J.; Lutz, M.; Spek, A. L. Two pyrazolato-bridged, linear trinuclear Cu(II) complexes. Crystal structures and magnetic properties. *Inorg. Chim. Acta* **2003**, *350*, 25-31.

FOR TABLE OF CONTENTS ONLY: